Additive Manufacturing 16 (2017) 153–161

Contents lists available at ScienceDirect

Additive Manufacturing

journal homepage: www.elsevier.com/locate/addma

Full Length Article

A Tripropylene Glycol Diacrylate-based Polymeric Support Ink for Material Jetting

Yinfeng He*, Fan Zhang, Ehab Saleh, Jayasheelan Vaithilingam, Nesma Aboulkhair, Belen Begines, Chris J. Tuck, Richard J.M. Hague, Ian A. Ashcroft, Ricky D. Wildman

Faculty of Engineering, University of Nottingham, Nottingham, UK

ARTICLE INFO

Article history:
Received 6 September 2016
Received in revised form 3 May 2017
Accepted 11 June 2017
Available online 12 June 2017

Keywords:
Additive manufacturing
Inkjet printing
Material jetting
Support material
UV curing
TPGDA

ABSTRACT

Support structures and materials are indispensable components in many Additive Manufacturing (AM) systems in order to fabricate complex 3D structures. For inkjet-based AM techniques (known as Material Jetting), there is a paucity of studies on specific inks for fabricating such support structures. This limits the potential of fabricating complex 3D objects containing overhanging structures. In this paper, we investigate the use of Tripropylene Glycol Diacrylated (TPGDA) to prepare a thermally stable ink with reliable printability to produce removable support structures in an experimental Material Jetting system. The addition of TGME to the TPGDA was found to considerably reduce the modulus of the photocured structure from 575 MPa down to 27 MPa by forming micro-pores in the cured structure. The cured support structure was shown to be easily removed following the fabrication process. During TG-IR tests the $T_{5\%}$ temperature of the support structure was above 150 °C whilst the majority of decomposition happened around 400 °C. Specimens containing overhanging structures (gate-like structure, propeller structure) were successfully manufactured to highlight the viability of the ink as a support material.

1. Introduction

Additive Manufacturing (AM), colloquially known as 3D Printing (3DP), is a manufacturing approach that enables the fabrication of a 3D structure on a layer by layer basis, usually from a computer-generated file. The method has considerable advantages over traditional manufacturing, since it is free from the constraints of many subtractive or formative techniques. Over the last 25 years, it has moved from being used for prototyping purposes towards becoming an accepted manufacturing methodology [1–3]. The simplicity of the layer-by-layer approach, together with the freeform production methods that it offers, presents significant advantages in a wide range of fields, including biomedical, electronics and engineering structures [4–9]. Among the seven categories of AM techniques defined by the American Society for Testing and Materials (ASTM), Material Jetting (MJ) — '*an additive manufacturing process in which droplets of build materials are selectively deposited*' [10] — is particularly attractive due to its scalable production, potential for multi-material (and function) and high resolution [11–13]. Whilst there is much that is achievable with single material deposition, multi-material approaches can offer the opportunity for multifunctional components, combining for example, structural and biocompatible elements [14], electronics and diagnostics [15,16] and excipients and drugs [17].

Recent efforts in Material Jetting have demonstrated a widening vista of materials that can be processed [18–25]. However, several challenges present themselves. One of the most significant is the need for readily available materials that can support overhanging structures. Such supporting materials are needed since exploitation of the design freedoms afforded by AM often leads to the presence of cavities and voids. Material supports are an indispensable element, which work as a temporary base during fabrication and usually will be removed at the end of the process. Fahad et al. [25] suggested support materials need to support the layers of build material during the build process and be soft enough to be removed easily post fabrication. They hypothesised a methylcellulose-based ink, which could be used as a support material; [25]. Commercial 3DP inkjet companies have developed their own support structures, but their composition and use is usually protected. It is the aim of this paper to present alternative materials that are easy to

* Corresponding author.

http://dx.doi.org/10.1016/j.addma.2017.06.001

prepare, whilst also being inexpensive and effective, for the role of supports.

This paper focuses on the modification of Tripropylene Glycol Diacrylate (TPGDA) for the purposes of supporting structural materials during fabrication and post-manufacture removal. TPGDA is a commonly used material principally exploited for its balance of dielectric and structural properties [26], whilst also showing reliable jetting performance and good thermal stability. It is proposed that TPGDA can be mixed with Triethylene glycol methyl ether (TGME), a high boiling point solvent, in order to create a jettable support material. It will be demonstrated that the blending of TGME with TPGDA is akin to the formation of a hydrogel [27,28]; since the TGME solvent does not participate in the UV photochemistry that is used to crosslink TPGDA, this leads to the production of a soft gel-like structure. Evidence will be presented regarding the structural and thermal properties of the jetted materials and a demonstrator produced to illustrate that objects can be manufactured with this support.

2. Experimental

Formulations based on TPGDA with different proportions of TGME were prepared and their suitability for printing investigated. Rheological measurements were taken to determine printability and those formulations within the printable range were then printed using a Dimatix DMP-2830 in order to determine their behaviour during printing and after curing. Thermogravimetric Analysis coupled to Infrared Spectroscopy (TG-IR) and compression tests were used to evaluate their thermal and mechanical properties, respectively. Finally, demonstrators were built with a multi-head inkjet print system. These structures were used to illustrate that the use of the new support material enabled the fabrication of overhanging structures.

2.1. Ink preparation

Chemicals were all purchased from Sigma Aldrich and used as received. TPGDA (a mixture of isomers containing Mono Methyl Ether of Hydroquinone (MEHQ) and Hydroquinone (HQ) as inhibitors, technical grade) with 0 wt%, 10 wt%, 20 wt% and 30 wt% of TGME (95% purity) were mixed at room temperature with 2 wt% of 2, 4-diethylthioxanthone (DETX) and 2 wt% of Ethyl 4-(dimethylamino) benzoate (EDB), as photoinitiator and accelerator, respectively, in an amber vial. The mixture was then stirred at 800 rpm for 30 minutes to fully dissolve the initiators. The prepared inks were then degassed by bubbling nitrogen through them for 15 minutes to help minimize photoinhibition brought about by pre-dissolved oxygen.

2.2. Ejectability assessment

The viscosities of the ink candidates were measured in a Malvern Kinexus Pro equipped with a 40 mm parallel plate geometry and programmed with a shear rate table between 10 s^{-1} and 1000 s^{-1} at room temperature. The plate gap was set to 150 μm and each measurement was repeated three times. The surface tension of the droplet was measured by pendant droplet shape analysis (Kruss DSA 100S) [29], with each measurement repeated 5 times. The inverse Ohnesorge number or printing indicator, Z [30], was used to help judge the ejectability of the inks. Z is given by:

$$Z = \frac{\sqrt{\rho r \gamma}}{\mu} \quad (1)$$

where ρ is the density, r is the characteristic length (in this case the nozzle diameter), γ is the surface tension of the fluid and μ is the viscosity of ink at the printing temperature. A value of Z between 1 and 10 for a given ink suggests that it is ejectable by a drop-on-demand printhead.

2.3. Printing assessment

The ink candidates within the ejectable range were then printed with a Dimatix DMP-2830 material printer. The ink was injected into a print cartridge (DMC-11610) which was then fixed to a printhead consisting of 16 nozzles (21 μm in diameter). Stable droplets were obtained through adjustment of the pressure-generating waveform. A 365 nm UV LED unit was used to cure the deposited ink during printing through a free radical polymerization process.

2.4. SEM

The printed samples were put into liquid nitrogen and then fractured to expose the inner surfaces. The use of liquid nitrogen assists in minimising the potential polymer deformations induced by ductile fracturing. The sample was sputter coated with platinum at 2.2 kV for 90 seconds (Polaron SC7640) and then imaged using SEM (Hitachi TM3030).

2.5. TG-IR analysis

TG-IR analyses were carried out in an Evolved Gas Analyser TL 9000 (Perkin Elmer). A specimen of approximately 10 mg was cut from the printed sample for characterization while the heating rate was set to 40 °C per minute. The gas that was evolved during the temperature ramp was pumped from the TG into the IR module at a rate of 70 mL/min with a 150 °C tube temperature to prevent chemical condensation. Real-time infrared spectroscopy was performed to track the chemical species within the gas phase with a scanning interval of 2 cm^{-1} from 600 cm^{-1} to 4000 cm^{-1} and two scans per second.

2.6. Compression test

Cubic samples (5 mm edge length) were prepared for compression tests. The top and bottom sides of the samples were polished using SiC paper to ensure flat, parallel surfaces. An Instron Universal testing machine (Model 5969 Instron) was used with a load cell with a maximum available load of 5 kN. The compression tests were conducted in accordance with the ASTM standard D695. The crosshead speed during testing was 0.25 mm/min and the samples were loaded until fracture.

2.7. Demonstrator

A bespoke multi-material 3D Material Jetting system manufactured by Roth & Rau, encompassing six Spectra 128 SE print heads with Infrared and Ultra Violet (395 nm) processing methods was used to produce demonstrator components. In these experiments, one print assembly, which containing two printheads, was used and the inks was subsequently cured with the UV station (365 nm 1077 ± 8 mW/cm^2). One of the print heads was filled with a TPGDA based support ink and another with TPGDA-only ink as the structural material. Prior to multi-material fabrication, both the support ink and structural ink were printed independently and cured to measure their layer thickness after curing. These values were then used to inform the print strategy and calculate the number of layers required to achieve the designed dimensions. Gate-like and propeller structures were printed to demonstrate the feasibility of fabricating overhanging structures with the designed support ink.

Table 1
Physical properties and printing indicator of the ink candidates at room temperature.

TGME Proportion	Nozzle Diameter (μm)	Density (g/mL)	Viscosity (mPa s)	Surface tension (mN/m)	Z Parameter
0%	21	1.03	10.03 ± 0.03	30.78 ± 0.10	2.57
10%	21	1.03	8.94 ± 0.03	31.41 ± 0.11	2.92
20%	21	1.03	8.19 ± 0.04	31.13 ± 0.08	3.17
30%	21	1.03	7.19 ± 0.04	31.38 ± 0.04	3.62

(Density: TPGDA: 1.03 g/mL, TGME: 1.027 g/mL).

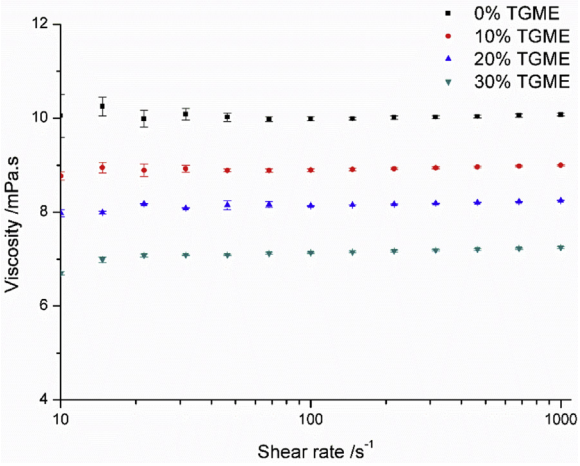

Fig. 1. Viscosity of the ink candidates with different TGME proportions at room temperature. Data are expressed as mean ± standard error, n = 3.

3. Results and Discussion

3.1. Ejectability Assessment

Viscosities of the ink candidates with different TGME proportions are shown in Fig. 1. All inks act as Newtonian fluids at 25 °C with viscosities ranging between 10 and 7 mPa s, depending on the TGME proportions. Viscosity, surface tension and density were measured (Table 1) for each of the ink candidates. After calculation of the *Z* parameter, results indicated that all the inks were within the ejectable range [6].

3.2. Printing

The inks were printed at 27 °C with a droplet spacing of 40 μm. The waveform shown in Fig. 2 was used to generate stable droplet formations with a peak printing voltage of 25 V. The droplet speed was 8 m/s, which was measured from images obtained directly from the print unit.

The appearance of the printed cubic samples fabricated with different ink candidates are shown in Fig. 3. Sagging of the printed ink was observed, especially for those with higher TGME concentrations. This causes morphological deviations between the printed samples and the original design. Sagging normally happens when the deposited ink droplet is not able to solidify instantly. The unsolidified or partially solidified fluid continues to spread and will neither be able to support itself nor any droplet deposited on to it. As more layers are printed, the sagging amplifies and will cause irregular, rounded edges [14]. Structures were not able to be constructed with inks containing more than 30% of TGME.

Table 2
The thermal properties of support structures fabricated with different inks measured by TGA.

TGME	Temperature (°C)		
	$T_{5\%}$	T_{max1}	T_{max2}
0%	308.54	N/A	403.82
10%	202.24	200.15	408.80
20%	157.78	196.62	403.85
30%	148.83	189.58	405.45

3.3. SEM

Fig. 4 shows the condition of the surface observed using SEM. As TGME proportion increased, submicron sized pores began to appear in the samples. Since TGME does not participate in the UV crosslink reaction, it is trapped inside the samples when the TPGDA cures. When the sample was cross-sectioned, the trapped TGME was exposed to the environment and evaporated during vacuum coating, leaving pores inside the samples. Fig. 4 also reveals that during the curing reaction, part of the TGME may precipitate out from the ink mixture and form a porous structure within the solidified structures.

3.4. TG-IR test of the thermostability

TG-IR enables the thermostability of the printed support structure to be assessed; this is an important attribute that is required within multimaterial, multifunctional inkjet printing due to the requirement to use heat curing or sintering mechanisms during fabrication (e.g., when printing functional conductive lines using nano-particulate inks [31–33]). Decomposition during this stage may lead to structural deformation, ultimately causing product failure.

TGA and differential thermogravimetry (DTG) curves of the fabricated samples are compared in Fig. 5. The relevant degradation data of $T_{5\%}$ (defined as the temperature at which the sample has 5% weight loss), T_{max1} and T_{max2} (the temperature at which the sample has maximum weight loss rate in stages 1 and 2, respectively) are given in Table 2.

It was observed that pure TPGDA had only one degradation stage occurring in the temperature range of 350–500 °C. For the supporting material, two stages of weight loss were detected. The first degradation stage occurs in the range of 150–250 °C which manifested weight losses of 10.5%, 22.5% and 31.5% for the ink with 10% 20% and 30% of TGME respectively. These weight losses correspond to the evaporation of TGME, which has a boiling point of 122 °C. The second stage, with a $T_{max2} \sim 400$ °C, could be attributed to the degradation of cured TPGDA which is generally observed to occur between 350 and 500 °C. Table 2 shows that as the proportion of TGME was increased, $T_{5\%}$ decreased reflecting the higher volumes of material available for evaporation.

The use of TG-IR allows the dynamic process of decomposition to be followed. The gas phase that evolved during each TG test was pumped into the IR detector and characterized in real-time allow-

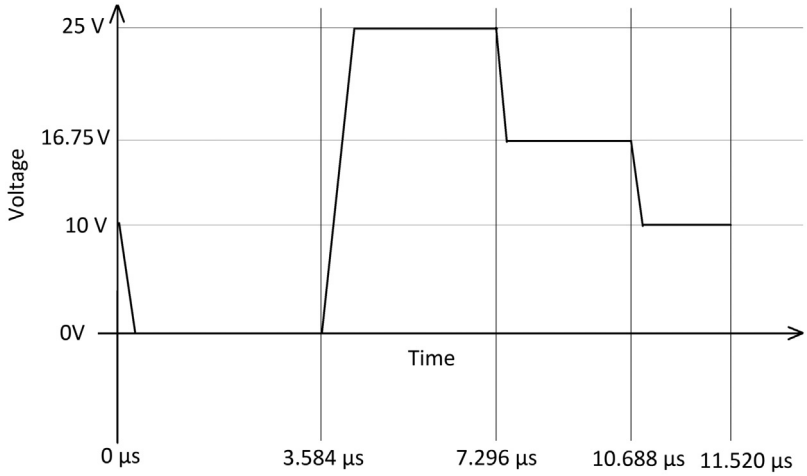

Fig. 2. Jetting waveform used perform printing on Dimatix.

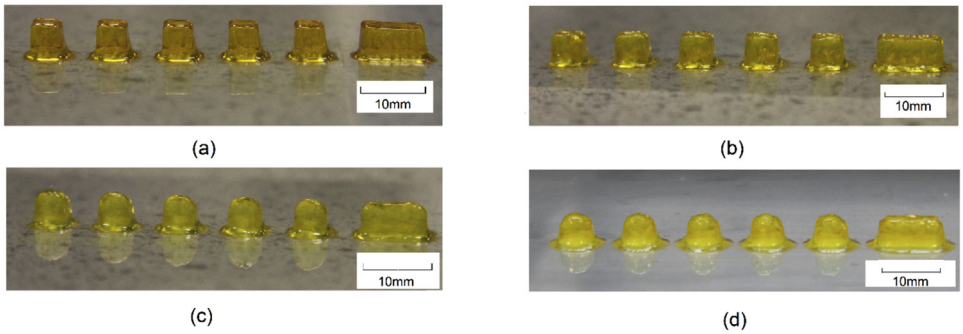

Fig. 3. Samples printed with different ink candidates through material jetting: (a) 0% TGME, (b) 10% TGME, (c) 20% TGME, (d) 30% TGME.

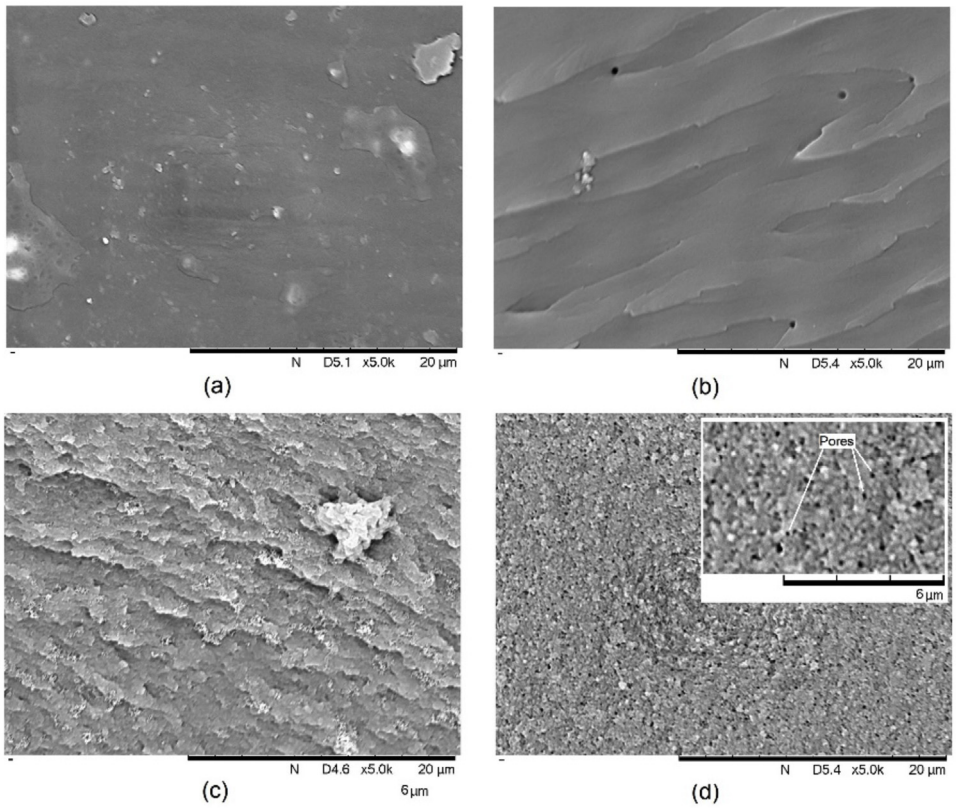

Fig. 4. SEM pictures of the printed samples' cross-section: (a) 0% TGME, (b) 10% TGME, (c) 20% TGME, (d) 30% TGME.

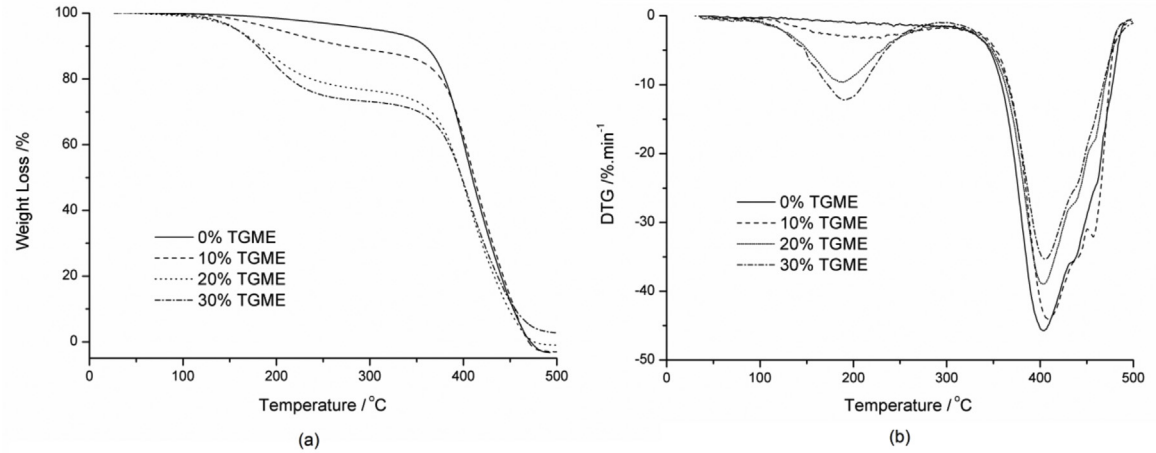

Fig. 5. (a) TGA and (b) DTG curves of printed support structures with different inks candidates.

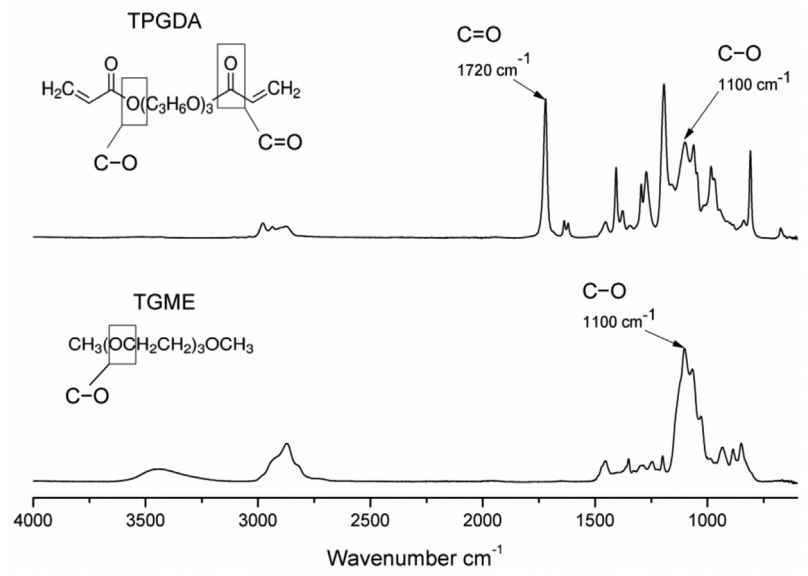

Fig. 6. FTIR absorbance spectra of TGME and TPGDA, the C—O bond with absorbance peak around 1100 cm^{-1} was used to track the degradation of both component and the C═O peak at 1720 cm^{-1} was used to distinguish the emission between TGME and TPGDA.

ing the tracking of the decomposition and evaporation during test. The C—O stretch peak at 1100 cm^{-1} was used to track the emission of TGME and TPGDA decomposition while the C═O stretch peak at 1720 cm^{-1} was used together with the C—O stretch peak to distinguish the emission of TGME and TPGDA decomposition (Fig. 6). By pairing the DTG curves with real-time IR peak intensities of the two identical peaks, it was chemically confirmed that the weight loss during the first degradation stage correlates with the evaporation of TGME and, the second stage, with the degradation of TPGDA (Fig. 7).

3.5. Compression Test

As TGME does not participate in the curing reaction, the lack of, for example, strong covalent bonding between TGME and TPGDA results in a fragile sample and a corresponding reduction in mechanical properties with increased levels of TGME. The compression tests showed that as the concentration of TGME increased from 0% to 30%, the Young's modulus significantly reduced from 575 MPa down to 27 MPa. Qualitatively, increases in TGME allowed for progressively easier removal of the support from the structural materials (Fig. 8 Table 3).

Table 3
Young's modulus of the printed support structures with different inks (mean ± standard error, n = 3).

TGME %	Young's modulus (MPa)
0	575 MPa ± 69
10	120 MPa ± 10
20	39 MPa ± 4
30	27 MPa ± 1

3.6. Demonstrators

A gate-like structure was printed (Fig. 9) to demonstrate the possibility of printing an overhanging structure. The average thickness of each layer of the structural ink and support ink were measured to be 4.5 μm and 6 μm respectively by measuring the thickness of

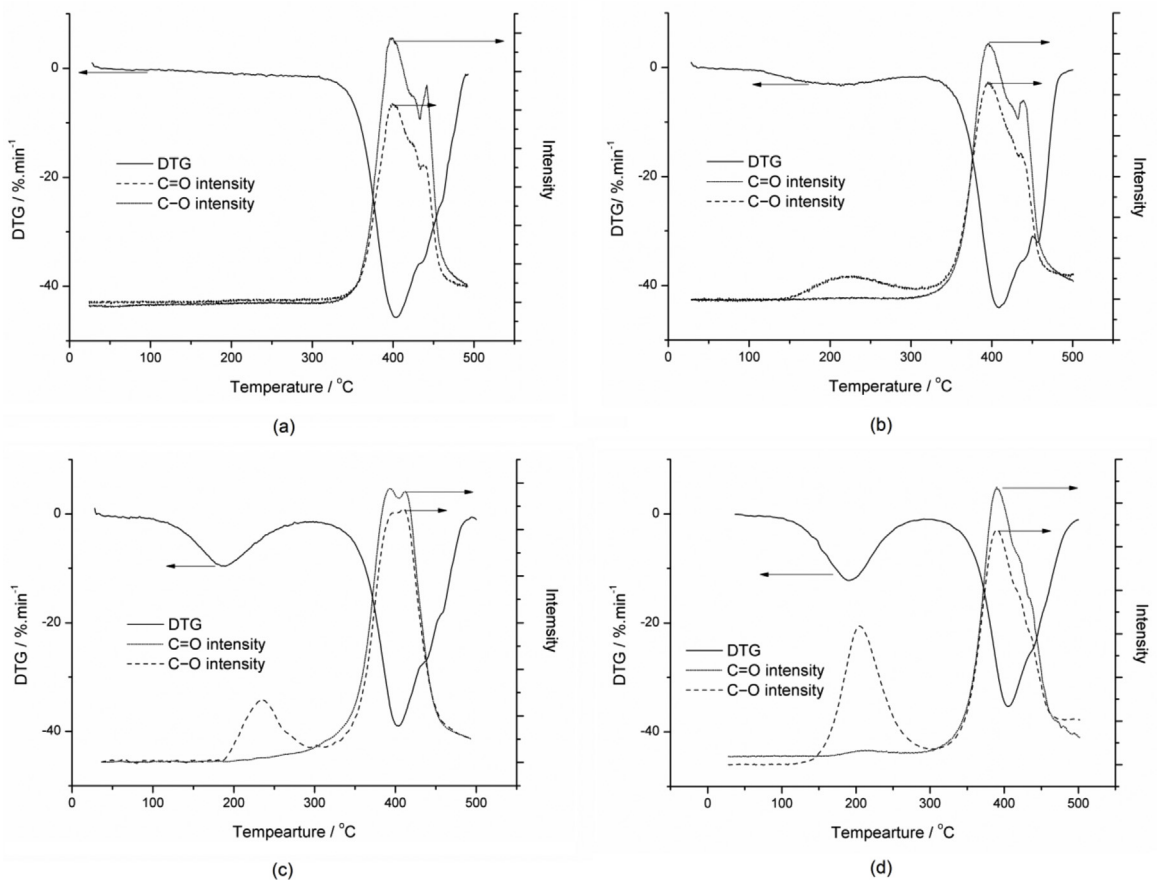

Fig. 7. TG-IR data of the support structures printed with different inks. The Derivative Thermogravimetric Analysis (DTG) data was correlated with the real-time IR gas phase analysis data to verify the emission's chemical composition during Thermal Gravimetric Analysis (TGA): (a) 0% TGME; (b) 10% TGME; (c) 20% TGME; (d) 30% TGME.

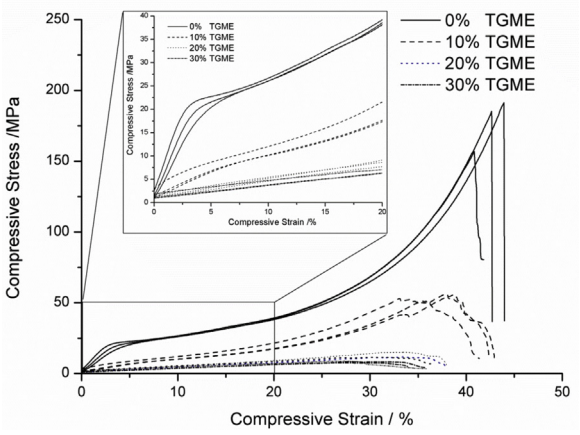

Fig. 8. Compression test of the supports printed with different ink formulations.

a 300 layer square structure through white light surface profiling. This layer thickness mismatch resulted in the need for more layers of the structural ink than the support to achieve a fixed height (Fig. 9(a) and (b)).

The support structure (Fig. 9, light yellow) can then be mechanically removed by tweezer or scalpel after fabrication (Fig. 9(d)). From Fig. 9 (c) and (d), it can be noted that with this simple approach of co-printing, even when there is compensation for layer thickness differences, small mismatches can result in amplified variances when many hundreds of layers are printed.

The dimensions of the printed gate-like structure were measured and compared to the design (Fig. 10). The printed specimen had ~5% deviation when compared to the intended design. The greatest deviations were observed across dimensions B and D (Fig. 10). This is most likely a result of slow curing, allowing spreading of droplets prior to fixing [14].

A more complex propeller structure, with significantly more overhanging regions, was also printed (Fig. 11). Despite the greater challenge and complexity, the variation was still found to be ~5% (Fig. 12), providing further evidence that the proposed formulation has potential as a 3D printing support material.

The roughness of the specimen surfaces was also characterized by white light surface profilometry in order to assess the quality of the interface between the structure and support material. R_z (mean roughness depth) was used to compare the surface quality and it was found that the surface of the structure material on top of the support was $R_a = 3.1 \pm 1.4\ \mu m$ (Fig. 12E) while at the interface between the support and structure material (Fig. 12F), the value of R_a was $12.4 \pm 2.6\ \mu m$. This indicates that the use of support material will increase the surface roughness, which could be induced by the interaction between the two surfaces as well as by the physical damage during the removal of support materials.

4. Conclusion

A TPGDA-based UV curable ink for support structure printing, which is easy to prepare, of low volatility and stable up to temper-

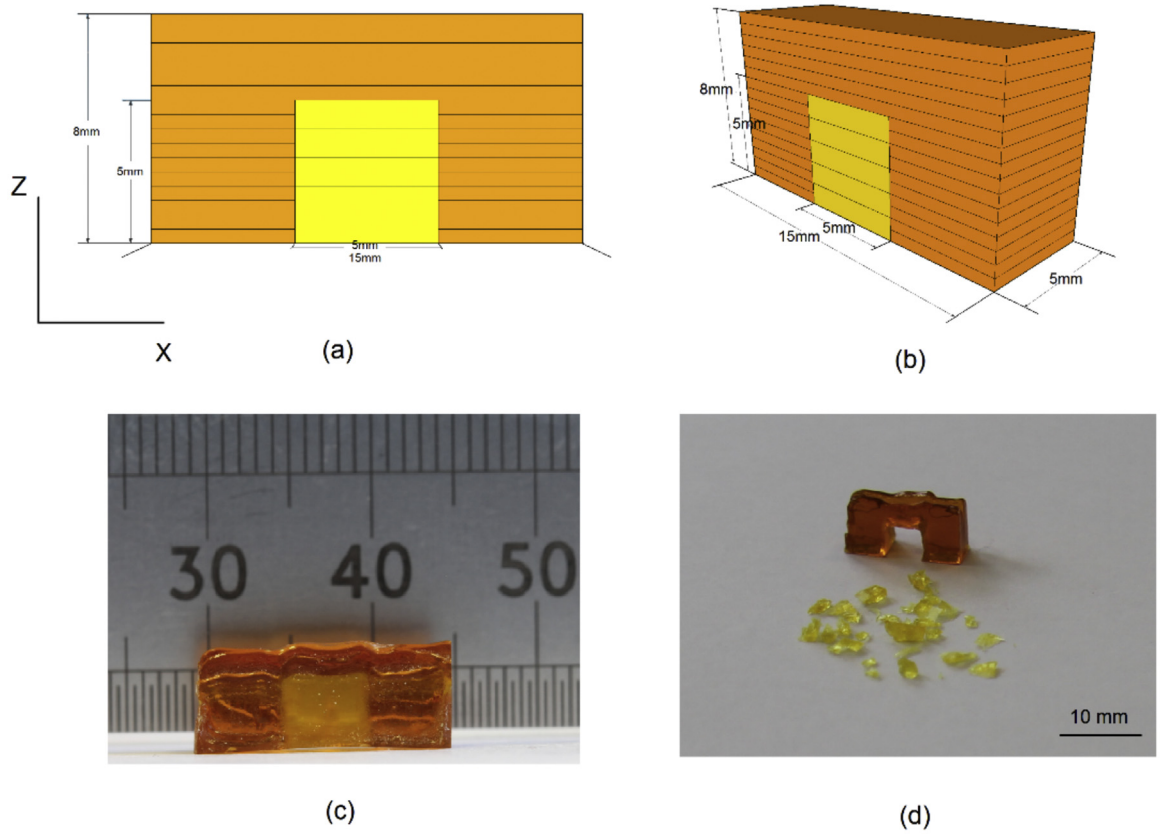

Fig. 9. (a) and (b): schematic of gate like structure; (c) front view of the printed demonstrator before the removal of support; (d) after the support structure was removed.

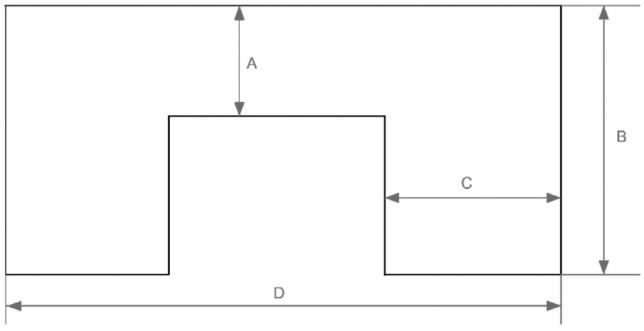

	Design (mm)	Printed (mm)
A	3	3.04±0.10
B	8	7.66±0.24
C	5	5.24±0.15
D	15	15.32±0.31

Fig. 10. comparison of dimensions between design and actual printed gate structure.

atures of around 150 °C, was printed and demonstrated. TGME was found to be an effective additive which can considerably reduce the mechanical properties of the cured TPGDA structure by forming a porous structure. The modulus reduced from 575 MPa down to 27 MPa with 30% of TGME. Gate-like and propeller demonstrators containing overhanging structures were printed with the developed support ink to illustrate the potential objects that could be manufactured with the help of the support ink. This ink formulation will allow the creation of more sophisticated geometries than that possible without supports. Inevitably, however, for highly complex, delicate or thin structures there are limitations to what a system based on mechanical removal can achieve and this simple approach may need other solutions, such as water soluble or chemically removable supports.

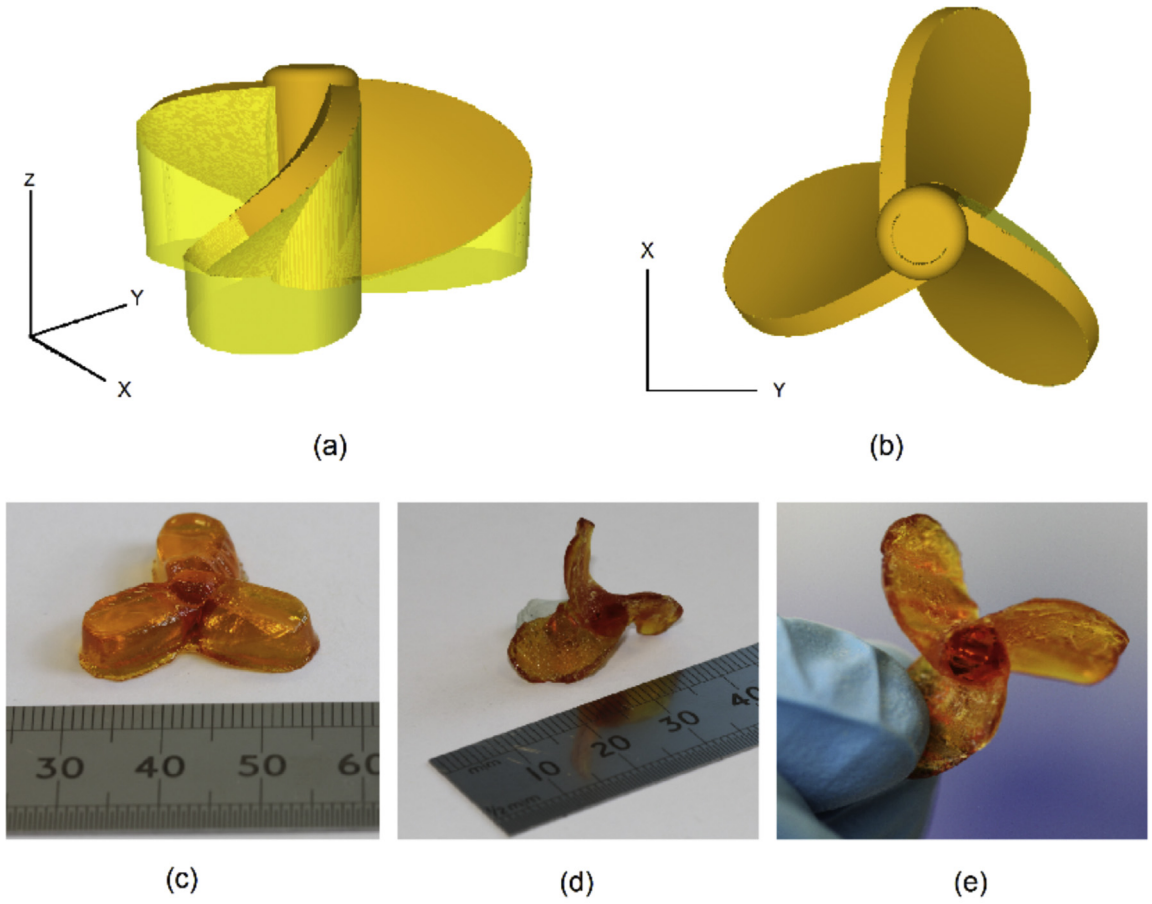

Fig. 11. A propeller structure fabricated with the help of prepared support ink (a) and (b): 3D model of the propeller structure with and without support; (c) print propeller with support; (d) and (e) after the removal of support structure.

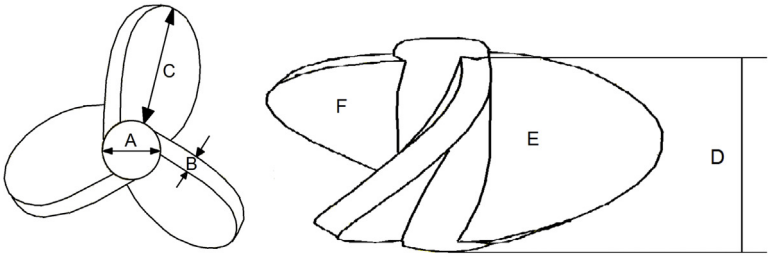

	Design (mm)	Printed (mm)
A	5	4.98±0.35
B	1.5	1.58±0.10
C	10.5	10.62±0.31
D	5	4.47±0.58

Fig. 12. comparison of dimensions between design and actual printed propeller.

Acknowledgements

This work was supported by the Engineering and Physical Sciences Research Council [grant number EP/I033335/2], "EPSRC Centre for Innovative Manufacturing in Additive Manufacturing", funded at the University of Nottingham.

References

[1] G.N. Levy, R. Schindel, J.P. Kruth, Rapid manufacturing and rapid tooling with layer manufacturing (LM) technologies, state of the art and future perspectives, CIRP Ann. Manuf. Technol. 52 (2) (2003) 589–609.
[2] R. Hague, I. Campbell, P. Dickens, Implications on design of rapid manufacturing, Proc. Inst. Mech. Eng. C: J. Mech. Eng. Sci. 217 (1) (2003) 25–30.

[3] K.K.B. Hon, L. Li, I.M. Hutchings, Direct writing technologies-advances and developments, CIRP Ann. Manuf. Technol. 57 (2008) 601–620.
[4] P. Krober, J.T. Delaney, J. Perelaer, U.S. Schubert, Reactive inkjet printing of polyurethanes, J. Mater. Chem. 19 (2009) 5234–5238.
[5] S.J. Hollister, Porous scaffold design for tissue engineering, Nature Mater. 4 (2005) 518–524.
[6] S.V. Murphy, A. Atala, 3D bioprinting of tissues and organs, Nature Biotechnol. 32 (2014) 773–785.
[7] S.J. Leigh, R.J. Bradley, C.P. Purssell, D.R. Bilson, D.A. Hutchins, A simple, low-cost conductive composite material for 3D printing of electronic sensors, PloS ONE 7 (11) (2012).
[8] R. Ramakrishnan, N. Saran, R.J. Petcavich, Selective inkjet printing of conductors for displays and flexible printed electronics, J. Disp. Technol. 7 (6) (2011) 344–347.
[9] P. Krober, J.T. Delaney, J. Perelaer, U.S. Schubert, Reactive inkjet printing of polyurethanes, J. Mater. Chem. 19 (2009) 5234–5238.
[10] ASTM, F2792, Standard Terminology for Additive Manufacturing Technology, ASTM International, 2012, available at: http:// www.astm.org.
[11] G.N. Levy, R. Schindel, J.P. Kruth, Rapid manufacturing and rapid tooling with layer manufacturing (LM) technologies, state of the art and future perspectives, CIRP Ann. Manuf. Technol. 52 (2) (2003) 589–609.
[12] I. Gibson, R.W. Rosen, B. Stucker, Additive manufacturing technologies: Rapid prototyping to direct digital manufacturing Ch.7, Springer, 2010, pp. 191–192.
[13] M. Ibrahim, T. Otsubo, H. Narahara, H. Koresawa, H. Suzuki, Inkjet printing resolution study for multi-material rapid prototyping, JSME Int. J., Ser. C 49 (2) (2006) 353–360.
[14] Y. He, C. Tuck, E. Prina, S. Kilsby, S.D.R. Christie, S. Edmondson, R.J.M. Hague, Rose FRAJ, R.D. Wildman, An new photocrosslinkable polycaprolactone based in for three-dimensional inkjet printing, J. Biomed. Mater. Res. B Appl. Biomater. (2016), http://dx.doi.org/10.1002/jbm.b.33699.
[15] C.A. Mirkin, T.A. Taton, Materials chemistry: semiconductors meet biology, Nature 405 (6787) (2000) 626–627.
[16] S.R. Nicewarner-Pena, R.G. Freeman, B.D. Reiss, et al., Submicrometer metallic barcodes, Science 294 (5540) (2001) 137–141.
[17] S.A. Khaled, J.C. Burley, M.R. Alexander, et al., Desktop 3D printing of controlled release pharmaceutical bilayer tablets, Int. J. Pharm. 461 (1) (2014) 105–111.
[18] B. de Gans, P.C. Duineveld, U.S. Schubert, Inkjet printing of polymers: state of the art and future development, Adv. Mater. 16 (3) (2004) 203–213.
[19] P. Calvert, Inkjet printing for materials and devices, Chem. Mater. 13 (2001) 3299–3305.
[20] E. Tekin, P.J. Smith, U.S. Schubert, Inkjet printing as a deposition and patterning tool for polymers and inorganic particles, Soft Matter 4 (2008) 703–713.
[21] C.J. Chang, Y.H. Lin, H.Y. Tsai, Synthesis and properties of UV-curable hyperbranched polymers for ink-jet printing of color micropatterns on glass, Thin Solid Films 519 (15) (2011) 5243–5248.
[22] Z. Fan, C. Tuck, R. Hague, Y. He, E. Saleh, Y. Li, C. Sturgess, R. Wildman, Inkjet printed polyimide film for capacitors, J. Appl. Polym. Sci. 133 (18) (2016).
[23] Gunasekera DHAT, S. Kuek, D. Hasanaj, Y. He, C. Tuck, A. Croft, R.D. Wildman, Three dimensional inkjet printing of biomaterials using ionic liquids and co-solvents, Faraday Discuss. (2016), http://dx.doi.org/10.1039/C5FD00219B.
[24] L.R. Hart, S. Li, C. Sturgess, R. Wildman, J.R. Jones, W. Hayes, 3D printing of biocompatible supramolecular polymers and their composites, ACS Appl. Mater. Interfaces 8 (5) (2016) 3115–3122.
[25] M. Fahad, P. Dickens, M. Gilbert, Novel polymeric support materials for jetting based additive manufacturing processes, Rapid Prototyp. J. 19 (4) (2013) 230–239.
[26] G. Abbas, Z. Ding, K. Mallik, H. Assemder, D.M. Taylor, Hysteresis-free vacuum-processed acrylate-pentacene thin-film transistors, IEEE Electron Device Lett. 34 (2) (2013) 268–270.
[27] J.L. Drury, D.J. Mooney, Hydrogels for tissue engineering: scaffold design variables and applications, Biomaterials 24 (24) (2003) 4337–4351.
[28] D. Myung, D. Waters, M. Wiseman, P.E. Duhamel, J. Noolandi, C.N. Ta, C.W. Frank, Progress in the development of interpenetrating polymer network hydrogels, Polym. Adv. Technol. 19 (6) (2008) 1–24.
[29] J.D. Berry, M.J. Neeson, R.R. Dagastine, D.Y.C. Chan, R.F. Tabor, Measurement of surface and interfacial tension using pendant drop tensiometry, J. Colloid Interface Sci. 454 (2015) 226–237.
[30] O. Basaran, Small-scale free surface flows with breakup: drop formation and emerging applications, AIChE J. 48 (9) (2002) 1842–1848.
[31] H.H. Lee, K.S. Chou, K.C. Huang, Inkjet printing of nanosized silver colloids, Nanotechnology 15 (10) (2005) 2436–2441.
[32] J. Perelaer, C.E. Hendriks, A.W.M. de Laat, U.S. Schubert, One-step inkjet printing of conductive silver tracks on polymer substrates, Nanotechnology 20 (2009) 1–5.
[33] T.H.J. van Osch, J. Perelear, A.W.M. de Laat, U.S. Schubert, Inkjet printing of narrow conductive tracks on untreated polymeric substrates, Adv. Mater. Commun. 20 (2008) 343–345.